

Bulk and surface switching in Mn-Fe-based Prussian Blue Analogues

T.T.A. Lummen,¹ R.Y.N. Gengler,¹ P. Rudolf,¹ F. Lusitani,¹ E.J.M. Vertelman^{1,2} P.J. van Koningsbruggen^{1,2} M. Knupfer,³ O. Molodtsova,³ J.-J. Pireaux,⁴ and P.H.M. van Loosdrecht^{1,*}

¹*Zernike Institute for Advanced Materials, University of Groningen,
Nijenborgh 4, 9747 AG Groningen, The Netherlands*

²*Stratingh Institute for Chemistry, University of Groningen,
Nijenborgh 4, 9747 AG Groningen, The Netherlands*

³*IFW Dresden, P.O. Box 270116, D-01171 Dresden, Germany*

⁴*L.I.S.E., Facultés Universitaires Notre-Dame de la Paix, Rue de Bruxelles 61, B-5000 Namur, Belgium*

(Dated: October 25, 2018)

Many Prussian Blue Analogues are known to show a thermally induced phase transition close to room temperature and a reversible, photo-induced phase transition at low temperatures. This work reports on magnetic measurements, X-ray photoemission and Raman spectroscopy on a particular class of these molecular heterobimetallic systems, specifically on $\text{Rb}_{0.97}\text{Mn}[\text{Fe}(\text{CN})_6]_{0.98} \cdot 1.03\text{H}_2\text{O}$, $\text{Rb}_{0.81}\text{Mn}[\text{Fe}(\text{CN})_6]_{0.95} \cdot 1.24\text{H}_2\text{O}$ and $\text{Rb}_{0.70}\text{Cu}_{0.22}\text{Mn}_{0.78}[\text{Fe}(\text{CN})_6]_{0.86} \cdot 2.05\text{H}_2\text{O}$, to investigate these transition phenomena both in the bulk of the material and at the sample surface. Results indicate a high degree of charge transfer in the bulk, while a substantially reduced conversion is found at the sample surface, even in case of a near perfect (Rb:Mn:Fe=1:1:1) stoichiometry. Thus, the *intrinsic* incompleteness of the charge transfer transition in these materials is found to be primarily due to surface reconstruction. Substitution of a large fraction of charge transfer active Mn ions by charge transfer inactive Cu ions leads to a proportional conversion reduction with respect to the maximum conversion that is still stoichiometrically possible and shows the charge transfer capability of metal centers to be quite robust upon inclusion of a neighboring impurity. Additionally, a 532 nm photo-induced metastable state, reminiscent of the high temperature $\text{Fe}^{\text{III}}\text{Mn}^{\text{II}}$ ground state, is found at temperatures 50-100 K. The efficiency of photo-excitation to the metastable state is found to be maximized 90 K. The photo-induced state is observed to relax to the low temperature $\text{Fe}^{\text{II}}\text{Mn}^{\text{III}}$ ground state at a temperature of approximately 123 K.

Keywords: Prussian Blue Analogues, Raman spectroscopy, XPS, Magnetic properties, charge transfer transitions, photo-induced transitions.

I. INTRODUCTION

In recent history, a substantial amount of scientific interest has been directed towards photomagnetic materials from a technological, application-oriented point of view, due to their favorable properties.¹ Among materials displaying photo-induced spin-crossover^{2,3,4,5,6} and valence tautomerism^{7,8,9,10,11}, an important subclass is formed by the so-called Prussian Blue Analogues. These molecular heterobimetallic coordination compounds exhibit intervalence charge transfer transitions induced by various external stimuli (temperature¹², pressure^{13,14}, visible light^{1,12} and X-rays.¹⁵) A prominent member of this subclass is $\text{Rb}_x\text{Mn}[\text{Fe}(\text{CN})_6]_{\frac{(2+x)}{3}} \cdot z\text{H}_2\text{O}$ ^{14,16,17,18}, which undergoes a temperature-induced charge transfer transition from a high temperature cubic lattice, space group $F\bar{4}3m$ (HT phase), to a low temperature tetragonal ($I\bar{4}m2$) phase (LT phase). This reversible, entropy-driven^{19,20} phase transition, which is described by $\text{Fe}^{\text{III}}(t_{2g}^5, S=1/2)\text{-CN-Mn}^{\text{II}}(t_{2g}^3e_g^2, S=5/2) \rightleftharpoons \text{Fe}^{\text{II}}(t_{2g}^6, S=0)\text{-CN-Mn}^{\text{III}}(t_{2g}^3e_g^1, S=2)$, occurs not only under the influence of temperature (HT \rightarrow LT at ~ 225 K, LT \rightarrow HT at ~ 290 K), but can also be induced by visible light irradiation at various temperatures^{16,20,21,22,25}, by hy-

drostatic pressure¹⁴ and possibly by X-ray radiation.¹⁵ In addition, these type of Prussian Blue Analogues have demonstrated a variety of other interesting properties such as a pressure-induced magnetic pole inversion²⁶ and multiferroicity²⁷. The capability of these materials to display switching phenomena, however, is known to depend rather crucially on its exact stoichiometry.^{17,20,23} Even though it has been established that the degree of conversion in these materials is maximized for systems closest to a Rb:Mn:Fe stoichiometry of 1:1:1, there appears to be an intrinsic limit to the maximum conversion achieved. To our knowledge, no $\text{Rb}_x\text{Mn}[\text{Fe}(\text{CN})_6]_{\frac{(2+x)}{3}} \cdot z\text{H}_2\text{O}$ system has ever been shown to undergo a complete transition from either configuration ($\text{Fe}^{\text{III}}\text{Mn}^{\text{II}}$ or $\text{Fe}^{\text{II}}\text{Mn}^{\text{III}}$) to the other. That is, all data on $\text{Rb}_x\text{Mn}[\text{Fe}(\text{CN})_6]_{\frac{(2+x)}{3}} \cdot z\text{H}_2\text{O}$ systems seem to indicate the presence of at least small amounts of the HT configuration ($\text{Fe}^{\text{III}}\text{Mn}^{\text{II}}$) when in the LT phase (configuration $\text{Fe}^{\text{II}}\text{Mn}^{\text{III}}$) and often also vice versa. The present understanding is that this incompleteness originates from the intrinsic local inhomogeneities of these materials, such as $\text{Fe}(\text{CN})_6$ -vacancies and alkali ion nonstoichiometry. This paper investigates where exactly the intrinsic incompleteness of the transition stems from in two ways: Firstly, by comparing the charge transfer (CT) properties of the bulk material to those of the surface material for both a 'near perfect' (close to 1:1:1 stoichiometry) sample and a less stoichiometric sample. Secondly, by quantitatively investigating the

effect of substituting part of the metal ions involved in the CT transition by CT-inactive ions. Three different samples, $\text{Rb}_{0.97}\text{Mn}[\text{Fe}(\text{CN})_6]_{0.98}\cdot 1.03\text{H}_2\text{O}$, $\text{Rb}_{0.81}\text{Mn}[\text{Fe}(\text{CN})_6]_{0.95}\cdot 1.24\text{H}_2\text{O}$, and $\text{Rb}_{0.70}\text{Cu}_{0.22}\text{Mn}_{0.78}[\text{Fe}(\text{CN})_6]_{0.86}\cdot 2.05\text{H}_2\text{O}$ are quantitatively compared utilizing different experimental techniques, which are all capable of distinguishing between the two configurations ($\text{Fe}^{\text{III}}\text{Mn}^{\text{II}}$ (HT) and $\text{Fe}^{\text{II}}\text{Mn}^{\text{III}}$ (LT)). Magnetic measurements are performed to obtain information on the bulk properties of the various samples, while XPS spectroscopy is used to extract the surface properties. Finally, Raman scattering is employed as a tertiary probe to investigate the materials' properties.

II. EXPERIMENTAL METHODS

A. Sample synthesis

All chemicals (of analytical grade) were purchased at Sigma-Aldrich and used without further purification. $\text{Rb}_{0.97}\text{Mn}[\text{Fe}(\text{CN})_6]_{0.98}\cdot 1.03\text{H}_2\text{O}$ (sample A) and $\text{Rb}_{0.81}\text{Mn}[\text{Fe}(\text{CN})_6]_{0.95}\cdot 1.24\text{H}_2\text{O}$ (sample B) are, respectively, samples 3 and 4 of a previous publication.²³ Their synthesis and detailed initial characterization can be found there. $\text{Rb}_{0.70}\text{Cu}_{0.22}\text{Mn}_{0.78}[\text{Fe}(\text{CN})_6]_{0.86}\cdot 2.05\text{H}_2\text{O}$ (sample C) was prepared similarly, by slowly adding a mixed aqueous solution (25mL) containing $\text{CuCl}_2\cdot 2\text{H}_2\text{O}$ (0.085 g, 0.02 M) and $\text{MnCl}_2\cdot 4\text{H}_2\text{O}$ (0.396 g, 0.08 M) to a mixed aqueous solution (25 mL) containing $\text{K}_3[\text{Fe}(\text{CN})_6]$ (0.823 g, 0.1 M) and RbCl (3.023 g, 1 M). The addition time was 20 minutes and the resulting solution was stirred mechanically and kept at a temperature of 50°C both during the addition time and for the subsequent hour. A brown powder precipitated. This was centrifuged and washed twice with distilled water of room temperature. The powder was allowed to dry in air for about 12 hours at room temperature. Yield (based on Mn + Cu): 81 %. Elemental analysis (details in Supporting Information) showed that the composition of sample C was $\text{Rb}_{0.70}\text{Cu}_{0.22}\text{Mn}_{0.78}[\text{Fe}(\text{CN})_6]_{0.86}\cdot 2.05\text{H}_2\text{O}$. X-ray powder diffraction showed that the sample was primarily (weight fraction 80.4(8) %) in the typical $F43m$ phase with the other fraction (19.6(8) %) in the $I4m2$ phase. The sample was confirmed to be single phase; phase separation into $\text{Rb}_x\text{Mn}[\text{Fe}(\text{CN})_6]_{\frac{(2+x)}{3}}\cdot z\text{H}_2\text{O}$ and $\text{Rb}_x\text{Cu}[\text{Fe}(\text{CN})_6]_{\frac{(2+x)}{3}}\cdot z\text{H}_2\text{O}$ fractions was excluded. See for details the Supporting Information. As noted in a previous paper²³, the samples under discussion here deviate from a perfect Rb:Mn(+Cu):Fe stoichiometry of 1:1:1. This deviation is ascribed to $[\text{Fe}(\text{CN})_6]^{3-}$ vacancies^{17,20,23} which are filled by H_2O molecules, consistent with the hydration found in the materials.

B. Instrumentation and measurement

Magnetic measurements. Magnetic measurements were performed on a Quantum Design MPMS magnetometer equipped with a superconducting quantum interference device (SQUID). Samples were prepared by fixing 20-30 mg of the compound (0.5 mg weight accuracy) between two pieces of cotton wool in a gelcap. For the magnetic susceptibility measurements of samples A and B, the samples were first slowly cooled from room temperature to 5 K (to ensure the samples are not quenched in their HT phase²⁴). Then the field was kept constant at 0.1 T while the temperature was varied from 5 K to 350 K and back to 150 K (rate ≤ 4 K/min.). For the magnetic susceptibility measurements of sample C the field was kept constant at 0.1 T while the temperature slowly varied from 330 to 5 K and back to 330 K.

X-ray photoemission spectroscopy. X-ray photoemission spectroscopy (XPS) data were collected at the IFW Leibniz Institute for Solid State and Materials Research in Dresden, using a SPECS PHOIBOS-150 spectrometer equipped with a monochromatic Al K_α X-ray source ($h\nu = 1486.6$ eV); the photoelectron take off angle was 90° and an electron flood gun was used to compensate for sample charging. The spectrometer operated at a base pressure of $1 \cdot 10^{-10}$ Torr. Evaporated gold films supported on mica served as substrates. Each powdered microcrystalline sample was dispersed in distilled-deionized water, stirred for 5 minutes, and a few drops of the resulting suspension were left to dry in air on a substrate. Directly after drying, the samples were introduced into ultra high vacuum and placed on a He cooled cryostat equipped with a Lakeshore cryogenic temperature controller to explore the 50-350 K temperature range. All binding energies were referenced to the nitrogen signal (cyanide groups) at 398 eV.²³ No X-ray induced sample degradation was detected. Spectral analysis included a Tougaard background subtraction²⁸ and peak deconvolution employing Gaussian line shapes using the WinSpec program developed at the LISE laboratory, University of Namur, Belgium.

Raman scattering. Inelastic light scattering experiments in the spectral region 2000-2300 cm^{-1} (the spectral region of the C-N stretching vibration) were performed in a 180° backscattering configuration, using a triple grating micro-Raman spectrometer (T64000-Jobin Yvon), consisting of a double grating monochromator (acting as a spectral filter) and a polychromator which disperses the scattered light onto a liquid N_2 cooled CCD detector. The spectral resolution was better than 2 cm^{-1} for the spectral region considered. Sample preparation was identical to that for XPS measurements and samples were placed in a liquid He cooled optical flow-cryostat (Oxford Instruments), where the temperature was stabilized with an accuracy of 0.1 K throughout the whole temperature range (from 300 to 50 K). A fraction of the second harmonic output of a Nd:YVO₄ laser (532.6 nm, Verdi-Coherent) was used as an excitation source and focused

on the samples using a 50x microscope objective (Olympus, N.A. 0.5). The power density on the samples was of the order of 600 W cm^{-2} .

III. RESULTS AND DISCUSSION

A. Magnetic susceptibility measurements

The inverse of the molar magnetic susceptibility, χ_M^{-1} , of the three samples is plotted in fig. 1, as a function of temperature. In all three samples the magnetic properties show a thermal hysteresis; when heating the sample from 5 K up, a decrease in χ_M^{-1} , accompanied by a decrease in the slope of the χ_M^{-1}, T -curve, occurs at a characteristic temperature $T_{1/2\uparrow}$, signaling the charge transfer (CT) transition from the $\text{Fe}^{\text{II}}\text{-CN-Mn}^{\text{III}}$ (LT) configuration to the $\text{Fe}^{\text{III}}\text{-CN-Mn}^{\text{II}}$ (HT) configuration. Subsequent cooling shows the samples undergoing the reverse transition at a temperature $T_{1/2\downarrow}$, which is significantly lower than $T_{1/2\uparrow}$. Temperatures $T_{1/2\uparrow}$ and $T_{1/2\downarrow}$ are defined as the temperatures at which half of the CT transition has occurred in the respective heating and cooling runs. Values of $T_{1/2\downarrow} = 240 \text{ K}$ and $T_{1/2\uparrow} = 297 \text{ K}$ for sample A ($\text{Rb}_{0.97}\text{Mn}[\text{Fe}(\text{CN})_6]_{0.98}\cdot 1.03\text{H}_2\text{O}$), $T_{1/2\downarrow} = 197 \text{ K}$ and $T_{1/2\uparrow} = 283 \text{ K}$ for sample B ($\text{Rb}_{0.81}\text{Mn}[\text{Fe}(\text{CN})_6]_{0.95}\cdot 1.24\text{H}_2\text{O}$) and $T_{1/2\downarrow} = 170 \text{ K}$ and $T_{1/2\uparrow} = 257 \text{ K}$ for sample C ($\text{Rb}_{0.70}\text{Cu}_{0.22}\text{Mn}_{0.78}[\text{Fe}(\text{CN})_6]_{0.86}\cdot 2.05\text{H}_2\text{O}$), as extracted from corresponding $\chi_M T$ -curves, yield hysteresis widths of 57, 86 and 87 K, respectively.

The magnetic properties of these samples are comparable to those reported for other $\text{Rb}_x\text{Mn}[\text{Fe}(\text{CN})_6]_{\frac{(2+x)}{3}}\cdot z\text{H}_2\text{O}$ compounds.^{17,20,23,29} The samples discussed here are consistent with the correlation between stoichiometry and hysteresis properties as found by Ohkoshi *et al.*¹⁷ and Cobo *et al.*²⁰ That is, with increasing amount of $\text{Fe}(\text{CN})_6$ vacancies, $T_{1/2\downarrow}$, $T_{1/2\uparrow}$ and the amount of Rb in the sample decrease, while $\Delta T = (T_{1/2\uparrow} - T_{1/2\downarrow})$ and the amount of H_2O in the sample increase. For all samples, the susceptibility of both the LT and HT phase was fit to Curie-Weiss behavior ($\chi_M^{-1} = \frac{(T - T_c)}{C}$), the corresponding fits are depicted by the blue (LT) and red (HT) lines in figure 1. Fits to the LT phase data were done in the temperature range from 20 K up to approximately 10 K below the respective $T_{1/2\uparrow}$ temperatures, while the fits to the data of the HT phases were done in the range from approximately 10 K above the respective $T_{1/2\downarrow}$ temperatures up to the maximum measurement temperature (325 K). From these fits we extracted the corresponding Curie constants (C), which are reported in table I. Theoretical values of the Curie constant, C , were calculated³⁰ for the assumed HT and LT phases of samples A ($\text{Rb}_{0.97}\text{Mn}[\text{Fe}(\text{CN})_6]_{0.98}\cdot 1.03\text{H}_2\text{O}$), B ($\text{Rb}_{0.81}\text{Mn}[\text{Fe}(\text{CN})_6]_{0.95}\cdot 1.24\text{H}_2\text{O}$) and C ($\text{Rb}_{0.70}\text{Cu}_{0.22}\text{Mn}_{0.78}[\text{Fe}(\text{CN})_6]_{0.86}\cdot 2.05\text{H}_2\text{O}$) and are

also given in table I. The fits also yielded the characteristic temperatures θ for all samples in both the HT and LT phases. Upon incorporation of ferromagnetic interactions in the system (present in the HT phase of sample C, where Fe^{III} and Cu^{II} ions interact ferromagnetically), one would expect to see a shift of the negative θ to smaller values (antiferromagnetic interactions remain dominant). Indeed, such a shift can be seen ($\theta = -7.7 \text{ K}$, -17.6 K and -6.2 K for sample A, B and C, respectively.). However, the θ values extracted from the HT fits are the result of an extrapolation over approximately 200 K, which would make the observed shift be within the expected error bars. The θ values corresponding to the LT fits do not show an obvious trend ($\theta = 9.6 \text{ K}$, 4.1 K and 6.5 K , respectively), which can be explained by the fact that in the LT the majority of the Fe ions have assumed the $S = 0$, Fe^{II} configuration. The result is that the ferromagnetic Mn-Mn interaction dominates the extracted parameters.

The theoretical C values calculated for sample A are, within the experimental accuracy, in good agreement with those obtained from the Curie-Weiss fit. In combination with the fact that in the calculations³⁰ all Fe ions and a stoichiometric amount of Mn ions were assumed to undergo the charge transfer (CT) transition in going from the HT to the LT configuration, these C values indicate that nearly all metal ions in sample A (which is very close to the 'perfect' 1:1:1 stoichiometry) undergo CT, resulting in a near maximum change in the magnetic properties. The calculated C value for the HT phase of sample B is slightly higher than the experimental value by about $0.3 \text{ emu K mol}^{-1}$. This might indicate that the sample contains trace amounts of magnetic impurities, which would increase the experimental C-value. The Curie constant calculated for the LT phase of sample B is also lower than its experimental value. Aside from aforementioned considerations, this difference can be explained by realizing that while the calculations assume a maximum possible degree of CT in the samples, this is not necessarily the case (Sample B deviates somewhat from the 1:1:1 stoichiometry). Thus, the difference can be ascribed to a fraction of the magnetic species not undergoing the CT transfer transition, even though the stoichiometry of the material would allow for it (i.e. excluding the magnetic species that do not undergo CT due to nonstoichiometry of Fe and Mn). This fraction will hereafter be referred to as the "inactive fraction" (IF) of the material. The estimated inactive fraction of each sample is also given in table I for both bulk (or more accurately, for bulk + surface material, as extracted from the magnetic measurements³¹) and surface material (as extracted from XPS spectra³¹ (vide infra)).

The Curie constants calculated for sample C are somewhat lower due to the partial substitution of Mn ions by Cu^{II} entities ($S = 1/2$) in the sample (the Cu ions are assumed to remain divalent at all temperatures, which is verified by the XPS measurements (vide infra)), the experimentally found value for the HT phase

TABLE I: Curie constants (C , emu K mol⁻¹) and 'inactive fractions' (IFs, see text) for all samples

Sample (phase)	C (exp.) ^a	C (calc.) ³⁰	IF (bulk, %) ^{b,31}	IF (surface, %) ^{b,31}
A (HT-phase)	4.87 ± 0.13	4.75	1 ± 1.9	72 ± 0.5
A (LT-phase)	3.04 ± 0.09	3.03 ^c	1 ± 1.9	72 ± 0.5
B (HT-phase)	5.03 ± 0.06	4.73	28 ± 1.1	65 ± 0.5
B (LT-phase)	3.53 ± 0.05	3.07 ^c	28 ± 1.1	65 ± 0.5
C (HT-phase)	3.65 ± 0.13	3.82	24 ± 0.8	78 ± 0.5
C (LT-phase)	2.78 ± 0.11	2.45 ^c	24 ± 0.8	78 ± 0.5

[1]Errors are mostly due to the uncertainty in the weight of the samples. This error is the same for both phases of a particular compound. The fitting error is of the order of 0.02 emu K mol⁻¹.

[2]The inactive fraction is defined as the fraction of the magnetic species not undergoing the CT transition, even though CT is stoichiometrically possible. I.e., the magnetic species that do not undergo CT due to Fe:Mn nonstoichiometry are excluded.

[3]The calculation of the C value requires assumptions on the degree of charge transfer in the compound. These calculated values correspond to the case of maximum stoichiometrically possible degree of conversion in each of the samples. See text for details.

is consistent with calculations. In the calculation of the Curie constant of the LT phase, all the Mn ions and the corresponding number of Fe ions were assumed to have undergone the CT transition. Whether or not a metal ion undergoes the CT transition in these systems is known, however, to depend on the local stoichiometry in the system.^{17,20,23} Therefore, the calculation, which effectively ignores the effect of the Cu ions on the CT probability of the other metal ions, is only a lower limit to the LT phase Curie constant, which corresponds to the case of maximum magnetic change across the transition for the given stoichiometry (Rb_{0.70}Cu_{0.22}Mn_{0.78}[Fe(CN)₆]_{0.86}·2.05H₂O) (i.e., assuming IF = 0 in the material). And indeed, the C -value found for the LT phase of sample B is somewhat larger than this calculated lower limit, as would be intuitively expected upon the incorporation of Cu ions into the lattice. For comparison, assuming a random distribution of the Cu ions on the Mn positions, the expected Curie constant for the LT phase would be 3.48 emu K mol⁻¹ (IF = 75.2 %) if only the Fe ions surrounded by 6 Mn ions (Fe[-CN-Mn]₆ clusters) are assumed to undergo the CT transition, 2.91 emu K mol⁻¹ (IF = 33.1 %) when also the Fe ions in a Mn₅Cu environment would transfer an electron and 2.50 emu K mol⁻¹ (IF = 3.5 %) when in addition even the Fe ions in Mn₄Cu₂ surroundings would undergo CT. The experimentally found C value (2.78 emu K mol⁻¹) indicates the magnetic properties are quite robust upon Cu-substitution; an estimated 76 % of the maximum possible CT transfer is still achieved (IF ≈ 24 %), which is even more than is the case for sample B (IF = ≈ 28 %). Moreover, it suggests the substitution of one (and possibly even two) Mn ion by a Cu ion in the Fe[-(CN)-Mn]₆ cluster does not 'deactivate' the CT-capability of the Fe-center, nor does it appear to reduce the cooperativity in the material, since the CT transition occurs in a similar short temperature interval

in all samples (see fig. 1).

B. X-ray Photoemission Spectroscopy (XPS).

XPS is a direct method for identifying the surface composition of a compound as well as the oxidation state of the various elements at the surface. Hence this technique is well suited to follow the phase transition as a function of temperature. Indeed, as the structural change of the compound is accompanied by a charge transfer between metallic ions, XPS will accurately quantify the corresponding changes in the oxidation states of the elements at the surface of the material.

Sample A (Rb_{0.97}Mn[Fe(CN)₆]_{0.98}·1.03H₂O). Figure 2 shows the Fe $2p_{3/2}$ core level photoemission spectrum of sample A at room temperature and at 140 K, as well as fits to the raw data. At both temperatures, the Fe $2p_{3/2}$ signal consists of three distinct contributions: the Fe^{II} line at 708.8 eV binding energy, the Fe^{III} line at 710.5 eV and the Fe^{III} satellite at 711.7 eV, the latter appearing 1.2 eV higher in binding than the Fe^{III} main line, having 30 % of its intensity.²³ By comparing the relative intensities of the Fe^{II} and Fe^{III} components in the room temperature spectrum, one deduces that the surface material of the compound is composed of 76 % Fe^{III} and 24 % Fe^{II}. No spectral changes are detected with respect to the room temperature data when slowly cooling the sample to 252 K (rate ~2 K/min., spectrum not shown here), just above the HT to LT phase transition (see figure 1). As previously mentioned, further cooling to 140 K induces a transition from the HT to the LT phase, accompanied by an electron transfer from the Mn^{II} to the Fe^{III} ions which is described as Fe^{III}(t_{2g}^5 , S=1/2)-CN-Mn^{II}($t_{2g}^3 e_g^2$, S=5/2) → Fe^{II}(t_{2g}^6 , S=0)-CN-Mn^{III}($t_{2g}^3 e_g^1$, S=2). The photoemission spectrum of the Fe $2p_{3/2}$ clearly qualitatively supports this transition, since the Fe^{III}/Fe^{II} ratio after the

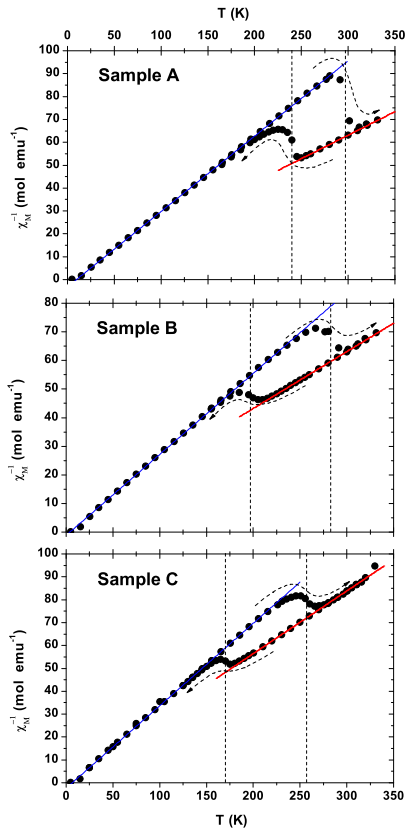


FIG. 1: χ_M^{-1} as a function of temperature for samples A ($\text{Rb}_{0.97}\text{Mn}[\text{Fe}(\text{CN})_6]_{0.98} \cdot 1.03\text{H}_2\text{O}$), B ($\text{Rb}_{0.81}\text{Mn}[\text{Fe}(\text{CN})_6]_{0.95} \cdot 1.24\text{H}_2\text{O}$) and C ($\text{Rb}_{0.70}\text{Cu}_{0.22}\text{Mn}_{0.78}[\text{Fe}(\text{CN})_6]_{0.86} \cdot 2.05\text{H}_2\text{O}$), showing the magnetic properties of the materials. The Curie-Weiss law was fitted to the data of both the HT and LT phases of the samples, the corresponding fits are indicated by the blue (LT) and red (HT) lines in the graphs. From the fits, experimental Curie constants (C) were extracted (see text). Dashed arrows indicate the temperature dependence of the data as measured in successive heating and cooling runs, while vertical indicate the corresponding transition temperatures.

transition is 48 %/52 %. However, the relative spectral intensities of the Fe^{III} and Fe^{II} components also show that the $\text{Fe}^{\text{III}} \rightarrow \text{Fe}^{\text{II}}$ conversion at the surface is far from complete (IF = 72 %), in contrast to the magnetic susceptibility measurements, which indicate a near complete conversion for the bulk (see also table I). This is explained by the surface sensitivity of the XPS technique, since the surface composition and structure can differ substantially from that of the corresponding bulk due to surface reconstruction. Thus, probing this surface stoichiometry using XPS shows the estimated³¹ inactive frac-

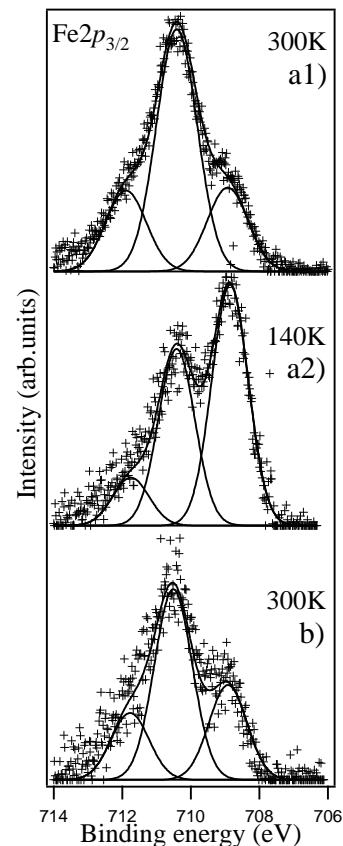


FIG. 2: $\text{Fe } 2p_{3/2}$ core level photoemission spectra of sample A ($\text{Rb}_{0.97}\text{Mn}[\text{Fe}(\text{CN})_6]_{0.98} \cdot 1.03\text{H}_2\text{O}$) collected at 300 and 140 K; fits to the raw data are depicted as solid lines. Spectra labeled a) are recorded during the cooling cycle, whereas the spectrum labeled b) refers to the measurement done after warming back up to 300 K. The binding energy scale is corrected for the temperature dependent shift (see text) for clarity.

tion of the surface material to be substantially larger in sample A.

Sample B ($\text{Rb}_{0.81}\text{Mn}[\text{Fe}(\text{CN})_6]_{0.95} \cdot 1.24\text{H}_2\text{O}$). The left panel of figure 3 shows the $\text{Fe } 2p_{3/2}$ core level photoemission spectrum (fits and raw data) of sample B for various temperatures, collected starting from 325 K, then while cooling to a minimum temperature of 50 K and successively warming up back to 325 K (cooling and warming rates both ~ 2 K/min.). As in the photoemission spectrum of sample A, the $\text{Fe } 2p_{3/2}$ signal consists of three distinct features: the Fe^{II} line at 708.8 eV binding energy, the Fe^{III} line at 710.5 eV and the Fe^{III} satellite at 711.7 eV. Additionally, a fourth small feature appears at the high binding energy side of the $\text{Fe } 2p_{3/2}$ signal. This contribution, which grows larger with decreasing temperature, is attributed to a contribution of the Fe^{II} shake up satellite. By comparing the relative $\text{Fe}^{\text{III}}/\text{Fe}^{\text{II}}$ intensity ratio for 325 K, 135 K and 50 K one observes the same trend as mentioned for sample A. The sample initially (at 325 K) consists of 85 % of Fe^{III} and 15 % of Fe^{II} and upon cooling, a decrease in the Fe^{III} peak intensity is ob-

served, whereas the Fe^{II} peak intensity simultaneously increases, consistent with the charge transfer between Fe^{III} and Mn^{II} ions. Spectra recorded at 135 K and 50 K both reveal similar $\text{Fe}^{\text{III}}/\text{Fe}^{\text{II}}$ ratios, namely 51 %/49 % and 50 %/50 %, respectively, in qualitative agreement with the magnetic susceptibility measurements (figure 1). As for sample A, quantitative differences are due to the surface sensitivity of the XPS technique and the increased inactive fraction of the surface material with respect to that of the bulk (~ 72 % vs. ~ 28 %, respectively).

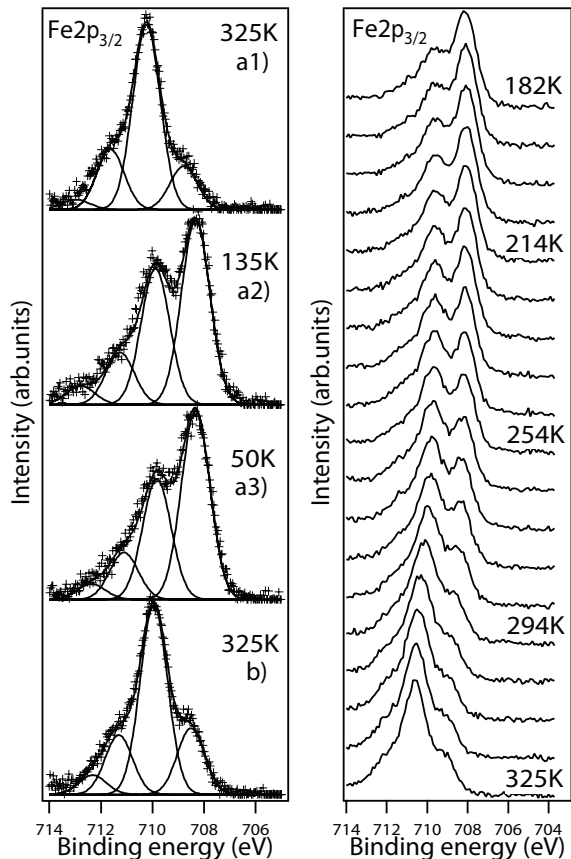


FIG. 3: Left panel: $\text{Fe } 2p_{3/2}$ core level photoemission spectra of sample B ($\text{Rb}_{0.81}\text{Mn}[\text{Fe}(\text{CN})_6]_{0.95} \cdot 1.24\text{H}_2\text{O}$) collected at 325, 135 and 50 K; solid lines depict fits to the raw data. Spectra labeled a) are recorded during the cooling cycle, whereas the spectrum labeled b) refers to the measurement done after warming back up to 325 K. The binding energy scale is corrected for the temperature dependent shift (see text) for clarity. The right panel shows the evolution of the $\text{Fe } 2p_{3/2}$ core level photoemission spectrum as sample B is warmed up from 182 to 325 K. Consecutive spectra are ~ 8 K apart. The binding energy scale is not rescaled here.

In order to visualize the continuous conversion across the CT transition in the surface material, we also recorded a series of $\text{Fe } 2p_{3/2}$ spectra while slowly warming up the sample at a constant rate (~ 3.5 K/min.). The right panel of figure 3 shows this sequence starting at 182 K and reaching 325 K with a temperature step of ~ 8 K between spectra. The series clearly shows a continuous

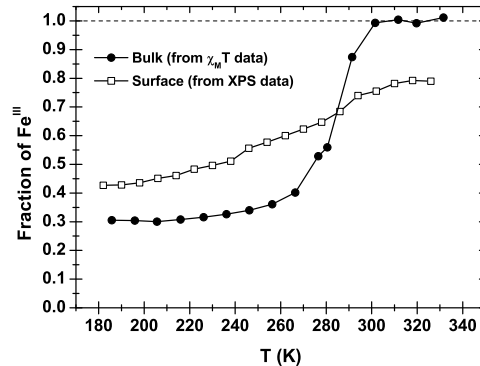


FIG. 4: Comparison between Fe^{III} fractions in bulk and surface material of sample B when heated through the CT transition. Bulk data (estimated from $\chi_M T$ values) shows a much larger conversion fraction across a rather abrupt transition, whereas surface data (as extracted from XPS spectra) shows a substantially smaller and smooth conversion.

conversion from the LT to the HT configuration, testified to by the steadily decreasing intensity of the Fe^{II} peak and the increasing Fe^{III} spectral intensity. Thus, in contrast to the bulk material, the surface material undergoes a smooth transition from the HT to the LT phase, becoming progressively $\text{Fe}^{\text{III}}\text{Mn}^{\text{II}}$ due to the charge transfer from Fe^{II} to Mn^{III} ions (see also fig. 4). In the right panel of figure 3 a slight shift of the $\text{Fe } 2p_{3/2}$ peak toward higher binding energy is observed when increasing the temperature. A similar binding energy shift is observed for the Mn spectra (not shown). Comparable shifts were observed for all samples and cannot simply be attributed to sample charging since the Rb and Fe shifts occur in opposite directions. These shifts are due to a charge delocalization in the CN vicinities.³²

To illustrate the large differences between surface and bulk behavior across the CT transition, the fraction of Fe^{III} versus temperature is plotted in figure 4 for both bulk and surface material of sample B, during a heating process. Data for the bulk curve are estimated from corresponding $\chi_M T$ values, using the same formula as was used to calculate Curie constants.³⁰ Data for the surface curve are extracted from the XPS spectra of the warming sequence in the right panel of figure 3. The figure nicely visualizes the differences: bulk material shows a high degree of conversion (IF ~ 28 %) and displays a rather abrupt transition, while surface material shows a much smoother transition of a substantially lower amount of Fe ions. Also, neither the HT phase nor the LT phase of the surface material consists of only one configuration ($\text{Fe}^{\text{III}}\text{Mn}^{\text{II}}$ or $\text{Fe}^{\text{II}}\text{Mn}^{\text{III}}$). The differences are attributed to a strongly increased degree of disorder and inhomogeneity at the surface of the material, which increases the inactive fraction and effectively eliminates cooperativity between the metal centers, resulting in a smooth

transition across a broad temperature range.

Sample C ($\text{Rb}_{0.70}\text{Cu}_{0.22}\text{Mn}_{0.78}[\text{Fe}(\text{CN})_6]_{0.86}\cdot 2.05\text{H}_2\text{O}$). The left panel of figure 5 shows the Fe $2p_{3/2}$ core level photoemission spectrum (fits and raw data) of sample C for six temperatures, recorded during cooling down from 325 K to 50 K and subsequent warming up back to 325 K. As in samples A and B discussed above, the Fe $2p_{3/2}$ signal of sample C consists of the same three distinct features; the Fe^{II} line at 708.8 eV, the Fe^{III} line at 710.5 eV and the Fe^{III} satellite at 711.7 eV. What distinguishes sample C from the others is the fact that it contains $\approx 22\%$ of copper on the Mn positions. As expected, due to the inclusion of Cu into the lattice, sample C (fig. 5) shows a lower absolute Fe^{III} to Fe^{II} surface conversion in comparison to samples A and B: starting out from 77 % Fe^{III} and 23 % Fe^{II} at 325 K, the sample shows a minimum ratio of 57 % Fe^{III} and 43 % Fe^{II} at 50 K. Comparison of the surface inactive fractions (in which the maximum degree of CT that is stoichiometrically possible is taken into account) however, shows the degree of conversion not to be anomalous (see table I). As for the previous two samples A and B, the surface IF is much higher than the corresponding bulk IF ($\sim 78\%$ vs. $\sim 24\%$), showing that also for sample C the phase transition is far from complete at the surface of the sample.

Additional information about the role of Cu comes from the Cu $2p_{3/2}$ core level photoemission data shown in the right panel of figure 5. One observes that the main peak at 935 eV³³ remains constant in intensity and binding energy throughout the temperature loop, revealing that the chemical environment of the copper does not change across the phase transition. One can therefore conclude that copper is not involved in the charge transfer process.

C. Raman Spectroscopy.

Inelastic light scattering is employed in order to indirectly determine the electronic and magnetic properties of the materials by addressing the vibrational stretching mode of its CN-moieties. In fact, the frequency of this vibrational mode, ν_{CN} , is highly sensitive to the local environment of the CN-moiety. Upon coordination, ν_{CN} will typically shift from its unbound ion frequency, 2080 cm^{-1} , to a higher frequency, characteristic of the local environment.³⁴ The extent of this shift is dependent on the electronegativity, valence and coordination number of the metal ion(s) coordinated to the CN-group and whether they are coordinated to the C or the N atom. Table II shows the typical frequency ranges where different CN stretching modes are expected to be observed, when the cyano-moiety is in a bimetallic bridge (an Fe-CN-M environment, where M = 3d metal ion). The given frequency ranges are estimates based on literature and experimental data of materials containing the specific or closely related CN-environments (varying the N-bound

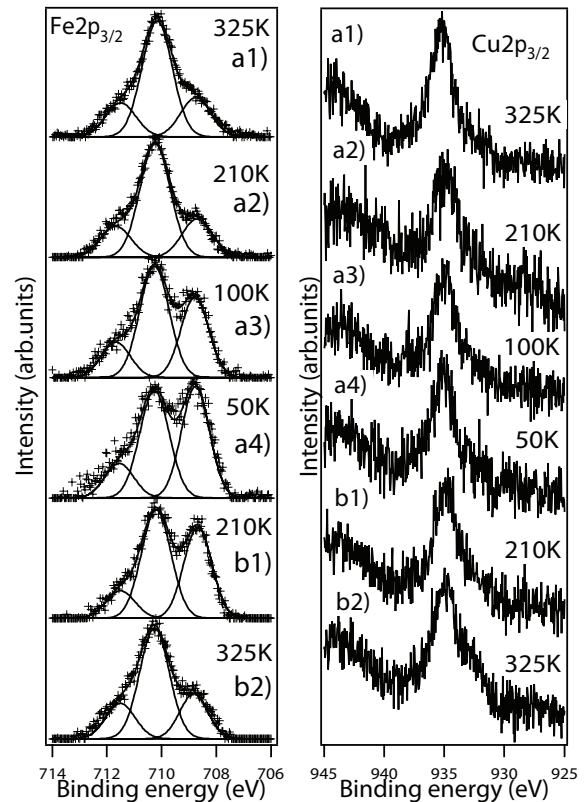


FIG. 5: Left panel: Fe $2p_{3/2}$ core level photoemission spectra of sample C ($\text{Rb}_{0.70}\text{Cu}_{0.22}\text{Mn}_{0.78}[\text{Fe}(\text{CN})_6]_{0.86}\cdot 2.05\text{H}_2\text{O}$) collected at 325, 210, 100 and 50 K. Solid lines depict fits to the raw data. Spectra indicated with an a) refer to measurements recorded during the cooling run, whereas spectra indicated with a b) were recorded during the subsequent heating run. The binding energy scale is corrected for the temperature dependent shift (see text) for clarity. Right panel: Corresponding Cu $2p_{3/2}$ core level photoemission spectra of sample C recorded at different temperatures during the same cooling and subsequent heating cycle.

metal ion).^{12,23,34,35,36,37} Across the thermal phase transition, in addition to the intervalence charge transfer, the $\text{Rb}_x\text{Mn}[\text{Fe}(\text{CN})_6]_{(2+x)/3}\cdot z\text{H}_2\text{O}$ lattice also contracts by approximately 10 %. This volume change decreases the average bond lengths in the system, thereby generally increasing the vibrational frequencies.

The Raman spectrum of all three samples at room temperature (in the HT phase) in the spectral window 2000-2250 cm^{-1} is shown in Fig. 6. Samples were heated to 330 K prior to measurements to ensure the samples were in their HT phase. Group theory analysis predicts that the vibrational stretching mode of the free CN^- ion (A_1 symmetry) splits up into an A_1 , an E and a T_2 normal mode, when the CN moiety is placed on the C_{2v} site of the $F\bar{4}3m (T_d^2)$ space group (the space group in the HT phase^{18,23,38,39}).

From the corresponding Raman tensors⁴⁰ it is clear that the A_1 , and E normal modes are expected to be observed in the parallel polarization spectra of figure

TABLE II: Specific frequencies and frequency ranges for CN stretching modes, ν_{CN} of CN-moieties in different environments in Prussian Blue Analogues (M = 3d metal ion).

CN-moiety	ν_{CN} (cm^{-1})
CN^- (aq)	2080 ³⁴
$\text{Fe}^{\text{II}}\text{-CN-Mn}^{\text{II}}$	2065 ³⁷
$\text{Fe}^{\text{II}}\text{-CN-Mn}^{\text{III}}$	2095, 2096, 2114 ^{12,20}
$\text{Fe}^{\text{II}}\text{-CN-Cu}^{\text{II}}$	2100 ³⁷
$\text{Fe}^{\text{II}}\text{-CN-Mn}^{\text{III}}$	2114 ²⁰
$\text{Fe}^{\text{III}}\text{-CN-Mn}^{\text{II}}$	2146, 2152, 2155, 2159, 2165, 2170 ^{12,20,23,37}
$\text{Fe}^{\text{III}}\text{-CN-Cu}^{\text{II}}$	2172 ^{23,37}
$\text{Fe}^{\text{II}}\text{-CN-M}^{\text{II}}$	2065-2100 ^{34,35,36,37}
$\text{Fe}^{\text{II}}\text{-CN-M}^{\text{III}}$	2090-2140 ^{12,23,34,36}
$\text{Fe}^{\text{III}}\text{-CN-M}^{\text{II}}$	2146-2185 ^{12,23,34,35,36,37}
$\text{Fe}^{\text{III}}\text{-CN-M}^{\text{III}}$	2180-2210 ^{34,35}

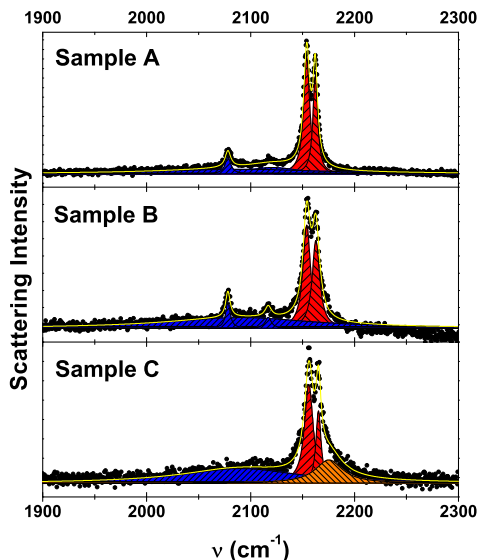


FIG. 6: Raman scattering spectra for all samples recorded at room temperature. Multiple lorentzian contributions (color filled peaks) were summed to obtain a fit (solid yellow line) to the data (black circles). Red peaks correspond to the HT configuration of the material ($\text{Fe}^{\text{III}}\text{-CN-Mn}^{\text{II}}$), while blue peaks represent the LT configuration ($\text{Fe}^{\text{II}}\text{-CN-Mn}^{\text{III}}$). The orange peak in the lowest panel (sample C) represents the CN-vibrations corresponding to $\text{Fe}^{\text{III}}\text{-CN-Cu}^{\text{II}}$ configurations.

6 (due to their non-zero diagonal tensor components). Indeed, all spectra show a double peak structure (red colored lines), with vibrations at 2156 and 2165 cm^{-1} , which are ascribed to the A_1 and E normal modes of the $\text{Fe}^{\text{III}}\text{-CN-Mn}^{\text{II}}$ (HT phase) moieties. These peaks are observed in the expected frequency range (see ta-

ble II) and are consistent with IR-data^{12,36,37} and previous Raman measurements.^{20,23,41} Also, the spectra of all samples show some additional Raman intensity at lower wavenumbers (blue colored lines), consistent with the presence of LT-configuration moieties ($\text{Fe}^{\text{II}}\text{-CN-Mn}^{\text{III}}$, table II), as was observed in the XPS data. In samples A and B, one can distinguish clear peak features at ~ 2080 and $\sim 2118 \text{ cm}^{-1}$ on top of the broad LT-phase intensity, whereas sample C shows only a featureless broad band. The presence of $\text{Fe}^{\text{III}}\text{-CN-Cu}^{\text{II}}$ cyano bridges in sample C is reflected in its spectrum through a shoulder on the high wavenumber side of the double peak structure (orange filled peak). The incorporation of Cu^{II} ions into the lattice is also evident in the width of the lines; inhomogeneous broadening as a result of the increased degree of disorder causes the peaks in sample C to be broader with respect to those in samples A and B, which is arguably also the reason the LT peak features are not distinguishable in sample C. Unfortunately, no reliable quantitative estimation regarding the $\text{Fe}^{\text{III}}/\text{Fe}^{\text{II}}$ ratios can be made from the intensities of the Raman lines, since these involve a phonon-dependent proportionality factor. In addition, possible photo-induced LT to HT switching at these temperatures would further complicate such estimations. Nonetheless, changes in the intensity of one phonon as a function of, for instance, temperature can give information on relative quantities of the given phonon.

Temperature dependence

Table II illustrates the effect of the variation of valence of either of the metal ions in an Fe-CN-M (cyano) bridge on the vibrational stretching frequency of the CN-moiety (ν_{CN}). The predominant trend is an increase in ν_{CN} with increasing oxidation state of either of the metal ions, where the valence of the C-bound metal ion appears to have a larger effect than that of the N-bound metal ion.^{34,42} Thus, across the temperature induced CT transition in these materials, when the local environment changes from $\text{Fe}^{\text{III}}\text{-CN-Mn}^{\text{II}}$ to $\text{Fe}^{\text{II}}\text{-CN-Mn}^{\text{III}}$ in the cooling run, a net downshift in vibrational frequencies is expected.

The evolution of the parallel polarization Raman spectrum of the three samples across the hysteresis range in a cooling run is shown in figure 7. At a temperature of 250 K , all samples still show the spectrum typical of the HT phase, which is discussed above. Upon cooling the samples through their respective CT transitions, however, the intensity of the HT (red) lines goes down and simultaneously, the intensity of the broad signal at lower wavenumbers increases and evolves into several new peaks at ~ 2202 , ~ 2125 , ~ 2108 , ~ 2089 and $\sim 2080 \text{ cm}^{-1}$ (blue lines). In addition, the HT lines are slightly shifted to higher frequencies, due to the contraction of the lattice. This suggests that, although no CT has occurred in the inactive fraction of the samples, the lattice does

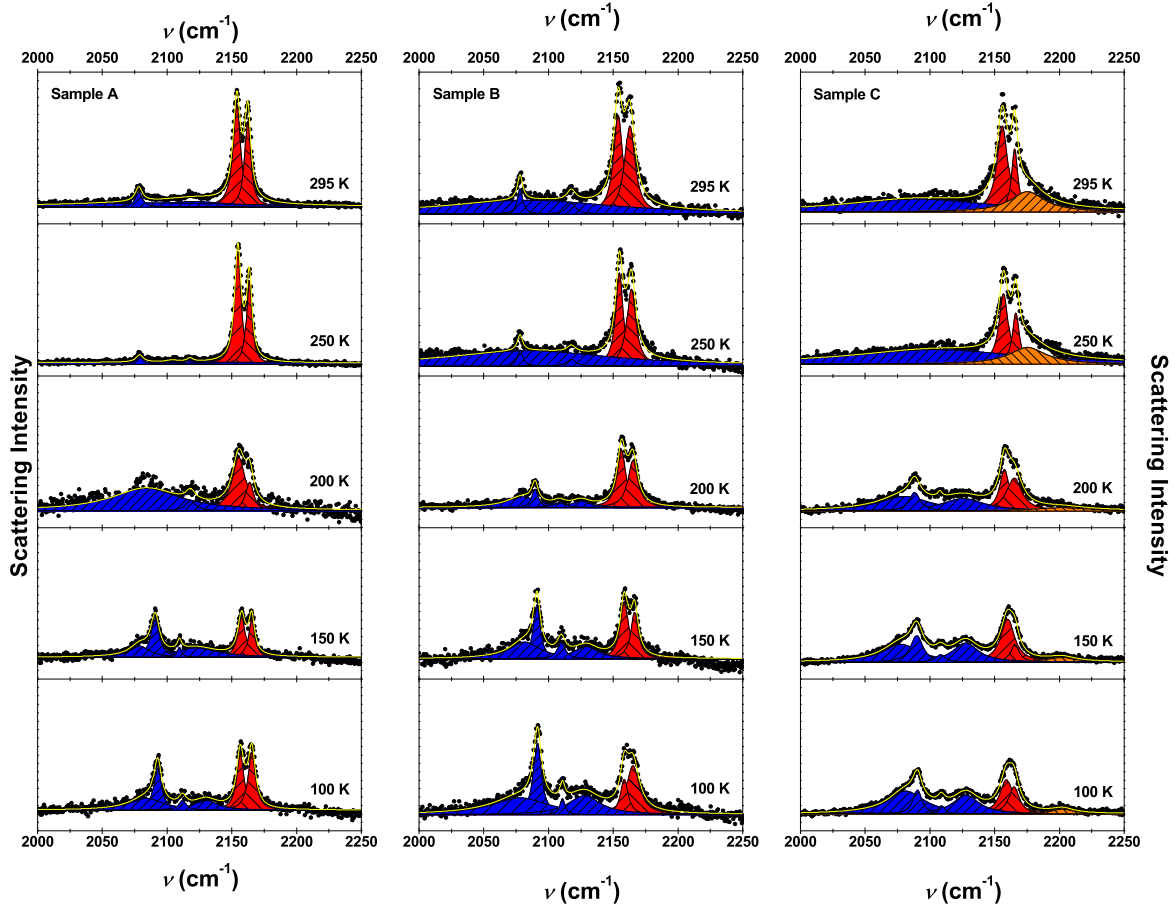


FIG. 7: Temperature dependence of the Raman spectrum of samples A ($\text{Rb}_{0.97}\text{Mn}[\text{Fe}(\text{CN})_6]_{0.98} \cdot 1.03\text{H}_2\text{O}$), B ($\text{Rb}_{0.81}\text{Mn}[\text{Fe}(\text{CN})_6]_{0.95} \cdot 1.24\text{H}_2\text{O}$) and C ($\text{Rb}_{0.70}\text{Cu}_{0.22}\text{Mn}_{0.78}[\text{Fe}(\text{CN})_6]_{0.86} \cdot 2.05\text{H}_2\text{O}$) across the hysteresis range in a cooling run. Multiple lorentzian contributions (color filled peaks, red = HT, blue = LT, orange = $\text{Fe}^{\text{III}}\text{-CN-Cu}^{\text{II}}$) were summed to obtain a fit (solid yellow line) to the data (black circles). Spectra are normalized to the total integrated scattering intensity in the $2000\text{-}2250\text{ cm}^{-1}$ window.

contract. Even though no quantitative $\text{Fe}^{\text{III}}/\text{Fe}^{\text{II}}$ ratio can be extracted from the Raman spectra, the presence of both HT (red) and LT (blue) lines seem to indicate an incomplete CT transition, in accordance with the XPS results. Consequently, multiple different Fe-CN-M environments are present in the LT phase of the samples, which explains the large number of lines observed in their Raman spectra. Next to the residual HT $\text{Fe}^{\text{III}}\text{-CN-Mn}^{\text{II}}$ configuration (red lines) and the LT $\text{Fe}^{\text{II}}\text{-CN-Mn}^{\text{III}}$ configuration, also $\text{Fe}^{\text{II}}\text{-CN-Mn}^{\text{II}}$ and $\text{Fe}^{\text{III}}\text{-CN-Mn}^{\text{III}}$ configurations are present in the LT phase. The latter configuration is confidently assigned to the 2202 cm^{-1} line, since it is the only configuration in which ν_{CN} is expected to increase (Table II). Less straightforward is the assignment of the other configurations since their cyano vibrations are expected to occur in overlapping frequency

ranges. In addition, the modes arising from these configurations are also expected to have split into multiple normal modes due to the crystal symmetry. For comparison, when assuming the space group $I4m2$ (that of $\text{Rb}_x\text{Mn}[\text{Fe}(\text{CN})_6]_{\frac{(2+x)}{3}} \cdot z\text{H}_2\text{O}$ in the LT phase^{18,23,38}), the CN vibrational mode splits up into 2 A_1 , a B_1 , a B_2 and an E mode, of which three (2 A_1 and B_1) would be observed in parallel polarization spectra. Nevertheless, based on the expected frequencies (table II) and the expected symmetry splitting the 2125 , 2108 and 2089 cm^{-1} lines are assigned to symmetry split normal modes of the $\text{Fe}^{\text{II}}\text{-CN-Mn}^{\text{III}}$ LT configuration, in agreement with Cobo *et al.*²⁰, while the 2080 cm^{-1} line is again tentatively assigned to the $\text{Fe}^{\text{II}}\text{-CN-Mn}^{\text{II}}$ configuration. Due to the fact that the $\text{Fe}^{\text{II}}\text{-CN-Mn}^{\text{II}}$ and $\text{Fe}^{\text{III}}\text{-CN-Mn}^{\text{III}}$ configurations occur at the interface between a metal ion that has and

a metal ion that has not undergone CT (generally in an environment with local inhomogeneities), the symmetry splitting of the modes assigned to these configurations is lost in the inhomogeneously broadened width of their corresponding lines (2080 and 2202 cm^{-1}). One may also expect the Raman spectrum of sample C in the LT phase to show vibrations arising from the $\text{Fe}^{\text{II}}\text{-CN-Cu}^{\text{II}}$ ($\approx 2100 \text{ cm}^{-1}$) and $\text{Fe}^{\text{III}}\text{-CN-Cu}^{\text{II}}$ ($\approx 2175 \text{ cm}^{-1}$) configurations, however, due to their low intensity and frequency overlap with more intense lines, it is not possible to resolve these lines in the present data. Overall, the temperature dependence of the Raman spectrum is in general good agreement with the XPS measurements, nicely demonstrating the temperature-induced CT transition. In addition to the changes in the vibrational spectra, all samples show a pronounced color change across the CT transition. The samples are substantially darker in their LT phase and are more susceptible to laser-induced degradation.

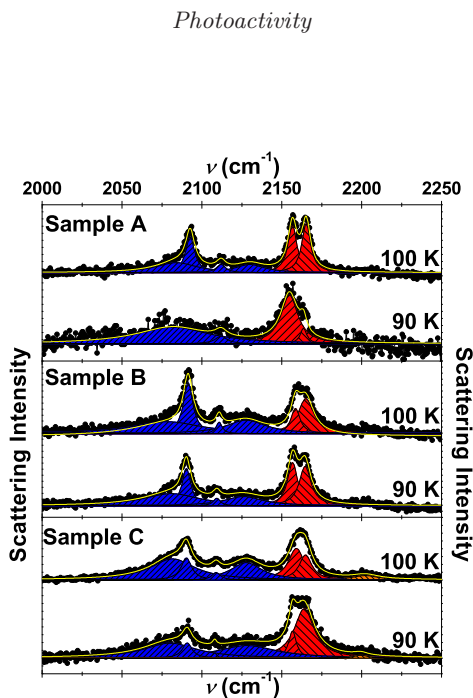


FIG. 8: Raman spectra of all three samples at 100 K and 90 K below the hysteresis in a cooling run. In all samples, the spectra at 90 K show an increase in intensity of the HT lines and a decrease of the LT lines with respect to the corresponding 100 K spectra. This is attributed to the photoactivity of the material (see text). All spectra are normalized to the total integrated scattering intensity in the 2000-2250 cm^{-1} spectral window

Remarkably, at a temperature of 90 K, the Raman spectra of the samples show the material has regained some intensity in the HT (red) lines at the cost of the LT (blue) lines (see fig 8), breaking the general trend of an increasing LT fraction with decreasing temperature.

Also, the double peak structure in sample C again shows a clear shoulder on the high frequency side, arising from the $\text{Fe}^{\text{III}}\text{-CN-Cu}^{\text{II}}$ cyano bridge. These features are explained in terms of the photoactivity of the material upon excitation of the sample using the Raman laser probe (532 nm). Around 90 K, $\text{Rb}_x\text{Mn}[\text{Fe}(\text{CN})_6]_{\frac{(2+x)}{3}} \cdot z\text{H}_2\text{O}$ has been shown to be photo-excited into a metastable state upon 532 nm laser excitation.^{20,22} The resulting metastable phase is described as 'HT-like', meaning that the predominant valence configuration is $\text{Fe}^{\text{III}}\text{-CN-Mn}^{\text{II}}$, which is consistent with the present and earlier²⁰ Raman spectra at these temperatures. A local laser induced heating effect is excluded, since the effect is not observed just below the corresponding hysteresis loops. Also, the metastable phase is stable in absence of laser irradiation and only relaxes to $\text{Fe}^{\text{II}}\text{-CN-Mn}^{\text{III}}$ ground state above a certain relaxation temperature (see below). In addition to the spectral changes, the sample is also observed to undergo a change in its optical properties under 532 nm excitation at this temperature: the excited material takes the substantially lighter HT appearance (the inverse of the color change seen when cooling through the CT transition). A similar effect is seen around 90 K: spectra recorded at 100, 80, 70, and 50 K also show increased intensity in the HT lines. The effect becomes increasingly less pronounced as the temperature deviates more from 90 K, which appears to be the temperature of maximum efficiency in photo-conversion. As the photo-conversion is accompanied by a color change, the (meta)stability of the photo-excited state is easily monitored visually, observing the sample color under a microscope. Consequently, the photo-excited 'HT-like' state was found to be persistent after excitation for at least 2 hours (without laser irradiation) at 90 K, showing no signs of relaxation to the darker LT ground state. During a subsequent slow heating ($\sim 0.5 \text{ K/min.}$) process the photo-excited state was visually monitored and found to relax to the LT ground state at a temperature of $\sim 123 \text{ K}$ (see movie clip in Supporting Information), consistent with the relaxation temperature reported by Tokoro *et al.*¹⁶ (120 K). A more elaborate study of the photo-conversion of the material as a function of temperature, excitation wavelength and intensity is required to elucidate the nature of this fascinating metastable photo-induced phase, the conversion mechanism involved and the striking temperature dependence of the effect.

IV. CONCLUSIONS

In conclusion, this work demonstrates the temperature-induced charge transfer transition in different Prussian Blue Analogue samples through a number of different experimental techniques, revealing the substantially reduced conversion factor of the surface material with respect to the bulk material. All three techniques, magnetic susceptibility measurements, XPS and Raman spectroscopy, show

the thermally induced charge transfer transition, which can be described as $\text{Fe}^{\text{III}}(t_{2g}^5, S=1/2)\text{-CN-Mn}^{\text{II}}(t_{2g}^3 e_g^2, S=5/2) \rightarrow \text{Fe}^{\text{II}}(t_{2g}^6, S=0)\text{-CN-Mn}^{\text{III}}(t_{2g}^3 e_g^1, S=2)$. Magnetic measurements indicate the bulk material shows a high degree of conversion (near maximal) in sample A ($\text{Rb}_{0.97}\text{Mn}[\text{Fe}(\text{CN})_6]_{0.98} \cdot 1.03\text{H}_2\text{O}$), while the conversion fraction is lower in sample B ($\text{Rb}_{0.81}\text{Mn}[\text{Fe}(\text{CN})_6]_{0.95} \cdot 1.24\text{H}_2\text{O}$). This is according expectation, as sample A is much closer to a Rb:Mn:Fe stoichiometry of 1:1:1. However, X-ray photoemission spectroscopy reveals a substantially lower HT \rightarrow LT conversion at the sample surface of all samples, the fraction of metal centers not undergoing the charge transfer transition is by far dominant at the surface, even in the highly stoichiometric sample A. This shows the *intrinsic* incompleteness of such systems to be due to surface reconstruction. Additionally, the CT transition is found to be much more smooth and continuous at the surface of the samples, due to the fact that cooperativity is effectively eliminated when the HT to LT conversion fraction is very low.

Though substitution of a fraction of the Mn^{II} ions by Cu^{II} ions (in sample C, $\text{Rb}_{0.70}\text{Cu}_{0.22}\text{Mn}_{0.78}[\text{Fe}(\text{CN})_6]_{0.86} \cdot 2.05\text{H}_2\text{O}$) is shown to reduce the degree of LT to HT conversion, the reduction is comparable to the fraction of Cu ions being substituted; for sample C ($\text{Rb}_{0.70}\text{Cu}_{0.22}\text{Mn}_{0.78}[\text{Fe}(\text{CN})_6]_{0.86} \cdot 2.05\text{H}_2\text{O}$), which contains 22 % of Cu on the Mn-positions, still 76 % of the maximum possible $\text{Fe}^{\text{III}}(t_{2g}^5, S=1/2)\text{-CN-Mn}^{\text{II}}(t_{2g}^3 e_g^2, S=5/2) \rightarrow \text{Fe}^{\text{II}}(t_{2g}^6, S=0)\text{-Mn}^{\text{III}}(t_{2g}^3 e_g^1, S=2)$ conversion is observed, which is comparable to the percentages found in sample B, which has no Cu incorporated in the lattice. Thus, the random substitution has little to no effect on the charge transfer capability

of individual metal clusters. In fact, a simple numerical analysis shows local $\text{Fe}[\text{-CN-Mn}]_5[\text{-CN-Cu}]$ and even $\text{Fe}[\text{-CN-Mn}]_4[\text{-CN-Cu}]_2$ clusters are not deactivated regarding charge transfer. Temperature dependent Raman spectroscopy is in agreement with above results, clearly displaying the charge transfer transition to be incomplete in all samples. Summarizing, these results show that the maximum total degree of HT \rightarrow LT conversion in these systems, found for highly stoichiometric samples is intrinsically limited by the fact that surface reconstruction deactivates metal clusters at the surface of the material regarding charge transfer.

At temperatures of 50-100 K, a remarkable photoactivity of the material is observed. Raman spectra in this temperature interval show the material to be photo-excited from the LT state, into a metastable "HT-like" state, meaning that the predominant valence configuration in this state is $\text{Fe}^{\text{III}}\text{Mn}^{\text{II}}$. This photo-conversion, which appears to be most efficient at 90 K, is accompanied by substantial color changes and is found to be stable below a relaxation temperature of ~ 123 K. How this state is related to the photo-excited (meta)stable phase at very low temperatures is not clear at the moment, further investigations are required to determine its exact nature and fascinating temperature dependence.

Acknowledgment. The authors would like to thank Roland Hubel for technical support during the XPS measurements at the IWF in Dresden. This work is part of the research programme of the 'Stichting voor Fundamenteel Onderzoek der Materie (FOM)', which is financially supported by the 'Nederlandse Organisatie voor Wetenschappelijk Onderzoek (NWO)'

* Electronic address: P.H.M.van.Loosdrecht@rug.nl

¹ Sato, O. *J. Photochem. Photobiol. C* **2004**, *5*, 203.

² Decurtins, S.; Güttlich, P.; Kohler, C. P.; Spiering, H.; Hauser, A. *Chem. Phys. Lett.* **1984**, *105*, 1.

³ Decurtins, S.; Güttlich, P.; Kohler, C. P.; Spiering, H. *Chem. Comm.* **1985**, *7*, 430.

⁴ Hauser, A.; Jeftić, J.; Romstedt, H.; Hinek, R.; Spiering, H. *Coordin. Chem. Rev.* **1999**, *190-192*, 471.

⁵ Güttlich, P.; Garcia, Y.; Goodwin, H. A. *Chem. Soc. Rev.* **2000**, *29*, 419.

⁶ Boillot, M.-L.; Zarembowitch, J.; Sour, A. *Spin Crossover in Transition Metal Compounds II*, (Springer, **2004**), vol. 234 of Top. Curr. Chem., p. 261.

⁷ Hendrickson, D. N.; Pierpont, C. G. *Spin Crossover in Transition Metal Compounds II*, (Springer, **2004**), vol. 234 of Top. Curr. Chem., p. 63.

⁸ Carducci, M. D.; Pressprich, M. R.; Coppens, P. *J. Am. Chem. Soc.* **1997**, *119*, 2669.

⁹ Caneschi, A.; Dei, A. *Angew. Chem. Int. Ed.* **1998**, *37*, 3005.

¹⁰ Carbonera, C.; Dei, A.; Letard, J.-F.; Sangregorio, C.;

Sorace, L. *Angew. Chem. Int. Ed.* **2004**, *43*, 3136.

¹¹ Carbonera, C.; Dei, A.; Sangregorio, C.; Sorace, L. *Chem. Phys. Lett.* **2004**, *396*, 198.

¹² Ohkoshi, S.-I.; Tokoro, H.; Hasmimoto, K. *Coord. Chem. Rev.* **2005**, *249*, 1830.

¹³ Ksenofontov, V.; Levchenko, G.; Reiman, S.; Güttlich, P.; Bleuzen, A.; Escax, V.; Verdaguer, M. *Phys. Rev. B* **2003**, *68*, 024415.

¹⁴ Morimoto, Y.; Hanawa, M.; Ohiski, Y.; Kato, K.; Takata, M.; Kuriki, A.; Nishibori, E.; Sakata, M.; Ohkoshi, S.; Tokoro, H.; Hashimoto, K. *Phys. Rev. B* **2003**, *68*, 144106.

¹⁵ Margadonna, S.; Prassides, K.; Fitch, A. N. *Angew. Chem. Int. Ed.* **2004**, *43*, 6316.

¹⁶ Tokoro, H.; Ohkoshi, S.-I.; Hashimoto, K. *Appl. Phys. Lett.* **2003**, *82*, 1245.

¹⁷ Ohkoshi, S.-I.; Matsuda, T.; Tokoro, H.; Hashimoto, K. *Chem. Mater.* **2005**, *17*, 81.

¹⁸ Kato, K.; Morimoto, Y.; Takata, M.; Sakata, M.; Umekawa, M.; Hamada, N.; Ohkoshi, S.; Tokoro, H.; Hashimoto, K. *Phys. Rev. Lett.* **2003**, *91*, 255502.

¹⁹ Luzon, J.; Castro, M.; Vertelman, E. J. M.; Gengler, R.;

- Broer, R.; van Koningsbruggen, P. J.; Rudolf, P.; van Loosdrecht, P. H. M. *J. Phys. Chem. A* **2008**, *112*, 5742.
- ²⁰ Cobo, S.; Fernández, R.; Salmon, L.; Molnár, G.; Bousseksou, A. *Eur. J. Inorg. Chem.* **2007**, *2007*, 1549.
- ²¹ Tokoro, H.; Matsuda, T.; Hashimoto, K.; Ohkoshi, S.-I. *J. Appl. Phys.* **2005**, *97*, 10M508.
- ²² Moritomo, Y.; Hanawa, M.; Ohishi, Y.; Kato, K.; Takata, M.; Kuriki, A.; Nishibori, E.; Sakata, M.; Ohkoshi, S.; Tokoro, H.; Hashimoto, K. *Phys. Rev. B* **2003**, *68*, 144106.
- ²³ Vertelman, E. J. M.; Maccallini, E.; Gournis, D.; Rudolf, P.; Bakas, T.; Luzon, J.; Broer, R.; Pugzlys, A.; Lummén, T. T. A.; van Loosdrecht, P. H. M.; van Koningsbruggen, P. J. *Chem. Mater.* **2006**, *18*, 1951.
- ²⁴ Tokoro, H.; Miyashita, S.; Hashimoto, K.; Ohkoshi, S.-I. *Phys. Rev. B* **2006**, *73*, 172415.
- ²⁵ Tokoro, H.; Matsuda, T.; Nuida, T.; Morimoto, Y.; Ohoyama, K.; Dangui, E. D. L.; Boukheddaden, K.; Ohkoshi, S.-I. *Chem. Mater.* **2008**, *20*, 423.
- ²⁶ Egan, L.; Kamenev, K.; Papanikolaou, D.; Takabayashi, Y.; Margadonna, S. *J. Am. Chem. Soc.* **2006**, *128*, 6034.
- ²⁷ Ohkoshi, S.-I.; Tokoro, H.; Matsuda, T.; Takahashi, H.; Irie, H.; Hashimoto, K. *Angew. Chem. Int. Ed.* **2007**, *46*, 3238.
- ²⁸ Tougaard, S. *J. Vac. Sci. Technol. A* **2005**, *23*, 741.
- ²⁹ Ohkoshi, S.-I.; Tokoro, H.; Utsunomiya, M.; Mizuno, M.; Abe, M.; Hashimoto, K. *J. Phys. Chem. B* **2002**, *106*, 2423.
- ³⁰ The theoretical C values were calculated using the formula $C = \frac{N_A \mu_B^2 g^2}{3k_B} \sum_i c_i S_i (S_i + 1)$, where N_A is Avogadro's number, μ_B is the Bohr magneton, g is the g-factor, taken as 2, S_i is the spin of the various transition metal ions in the sample, c_i is the corresponding stoichiometry coefficient of those ions (as given by the elemental analysis) and k_B is Boltzmann's constant. Assumed in the calculation for samples A and B was that all Fe-ions and the corresponding amount of Mn-ions undergo charge-transfer across the transition, the excess Mn-ions were assumed to remain in the bivalent, $S = 5/2$ state throughout the whole temperature range. In the case of sample C all Mn-ions and the corresponding amount of Fe-ions were assumed to undergo transfer (Since in this sample the Fe-ions outnumber the Mn-ions). Additionally, the Cu-ions were assumed to remain in their bivalent, $S = 1/2$ state at all temperatures. As the formula implies, the orbital momentum L was taken as 0 for the transition metal ions. Also, the g value is taken as 2.
- ³¹ The inactive fraction (IF) is defined as the fraction of the magnetic species not undergoing the ET transfer transition, even though ET is stoichiometrically possible. I.e., the magnetic species that do not undergo ET due to Fe:Mn nonstoichiometry are excluded. The estimated bulk IF values were calculated by matching the formula $C = \frac{N_A \mu_B^2 g^2}{3k_B} \sum_i c_i S_i (S_i + 1)$ (see reference above) to the experimental C -value of the corresponding LT phase. The estimated surface IF values are calculated from the experimental $\text{Fe}^{\text{III}}/\text{Fe}^{\text{II}}$ ratios extracted from corresponding XPS spectra. For sample C the IF is corrected for the material that is unable to undergo ET due to the $\#\text{Fe} > \#\text{Mn}$ nonstoichiometry.
- ³² Arrio, M.-A.; Sainctavit, P.; du Moulin, C. C.; Mallah, T.; Verdaguer, M.; Pellegrin, E.; Chen, C. T. *J. Am. Chem. Soc.* **1996**, *118*, 6422.
- ³³ Chawla, S. K.; Sankarraman, N.; Payer, J. H. *J. Electron Spectrosc. Relat. Phenom.* **1992**, *61*, 1.
- ³⁴ Nakamoto, K. *Infrared and Raman Spectra of Inorganic and Coordination Compounds*; Wiley-Interscience: New York, 4th ed., 1986.
- ³⁵ Reguera, E.; Bertrán, J. F.; Díaz, C.; Blanco, J.; Rondón, S. *Hyperfine Interact.* **1990**, *53*, 391.
- ³⁶ Sato, O.; Einaga, Y.; Fujishima, A.; Hashimoto, K. *Inorg. Chem.* **1999**, *38*, 4405.
- ³⁷ Bertrán, J. F.; Pascual, J. B.; Hernández, M.; Rodríguez, R. *React. Solids* **1988**, *5*, 95.
- ³⁸ Moritomo, Y.; Kato, K.; Kuriki, A.; Takata, M.; Sakata, M.; Tokoro, H.; Ohkoshi, S.-I.; Hashimoto, K. *J. Phys. Soc. Jpn.* **2002**, *71*, 2078.
- ³⁹ Moritomo, Y.; Kato, K.; Kuriki, A.; Takata, M.; Sakata, M.; Tokoro, H.; Ohkoshi, S.-I.; Hashimoto, K. *J. Phys. Soc. Jpn.* **2003**, *72*, 2698.
- ⁴⁰ Kuzmany, H. *Solid-State Spectroscopy - An Introduction*; Springer-Verlag: Berlin Heidelberg New York, 1998.
- ⁴¹ Vertelman, E. J. M.; Lummén, T. T. A.; Meetsma, A.; Bouwkamp, M. W.; Molnár, G.; van Loosdrecht, P. H. M.; van Koningsbruggen, P. J. *Chem. Mater.* **2008**, *20*, 1236.
- ⁴² Buschmann, W. E.; Enslin, J.; Güttlich, P.; Miller, J. S. *Chem. Eur. J.* **1999**, *5*, 3019.